Fusion and competing processes in the $^{32}S+^{12}C$ reaction at $E(^{32}S)=19.5$ MeV/nucleon

S. Pirrone,[1] G. Politi,[1,2] G. Lanzalone,[1] S. Aiello,[1] N. Arena,[1,2] Seb. Cavallaro,[1,2] E. Geraci,[2,3] F. Porto,[2,3] and S. Sambataro[1,2,†]

[1]*Istituto Nazionale di Fisica Nucleare–Catania, Corso Italia 57, I-95129 Catania, Italy*

[2]*Dipartimento di Fisica, Università di Catania, Corso Italia 57, I-95129 Catania, Italy*

[3]*Istituto Nazionale di Fisica Nucleare–Laboratori Nazionali del Sud, Via S. Sofia 44, I-95123 Catania, Italy*

(Received 21 July 2000; published 6 July 2001)

Velocity, angular, mass, and charge distributions of isotopically resolved residues coming from the reaction $^{32}S+^{12}C$ were measured at the bombarding energy $E(^{32}S)=19.5$ MeV/nucleon. Complete and incomplete fusion and direct components have been separated in the velocity spectra using kinematical analysis and deconvolution techniques. For each residue, incomplete and complete fusion cross sections have been extracted and the results are compared with the LILITA code predictions. The complete fusion cross section and the deduced critical angular momentum are also compared with other experimental data and with the predictions of theoretical models.

DOI: 10.1103/PhysRevC.64.024610 PACS number(s): 25.70.Jj

I. INTRODUCTION

The fusion reaction $^{32}S+^{12}C$ has been studied at energies between the Coulomb barrier and a few MeV/nucleon [1–4].

Experimental data [1] are relatively abundant in the literature at bombarding energies not far from the Coulomb barrier in the so-called [5] region I of the fusion excitation function, where the fusion cross section σ_{fus} is nearly equal to the total reaction cross section.

At higher energy (region II and region III of the excitation function) experimental data are less numerous [2–4] and the exact determination of the fusion cross section is complicated due to the presence of other competing processes, such as incomplete fusion, deep inelastic, and direct reactions. In particular, it has been suggested [6] that the fraction of incomplete fusion, with respect to the complete fusion, grows with the bombarding energy, while the fusion cross section decreases almost linearly with the inverse of the incident energy [7].

This trend can be attributed to a saturation of the critical angular momentum l_{cr} at a value l_{cr}^{max}, corresponding to the highest order partial wave contributing to the fusion cross section. Many theoretical approaches have been suggested to explain this behavior and they can be divided into two broad groups: the first one supports the idea of a fusion cross section limited by the entrance channel effects [8], while the second one attributes the limitation to compound nucleus properties [9,10].

In this paper, we present the results of a study on evaporation residues from the $^{32}S+^{12}C$ system at $E(^{32}S)=19.5$ MeV/nucleon; this energy falls within region III of the fusion excitation function, in which there is a complete lack of experimental data. Furthermore, we study the ratio between complete and incomplete fusion and provide new data related to the controversy about the fusion cross section limitation at higher incident energies.

The experimental procedure is described in Sec. II, while analysis of the experimental results is presented in Sec. III. Finally, the results obtained are discussed and compared to the predictions of some theoretical models in Sec. IV.

II. EXPERIMENTAL PROCEDURE

The experiment was performed at the superconducting cyclotron accelerator facility of the Laboratori Nazionali del Sud in Catania.

A beam of ^{32}S ions at an energy of 19.5 MeV/nucleon was collimated at the center of a scattering chamber on a ^{12}C target, of 460 $\mu g/cm^2$ nominal thickness. The target was placed perpendicular to the beam direction; its oxygen and the nitrogen contents were found to be negligible.

Isotopic identification of the reaction products, along with their energy and velocity measurements, was obtained by means of the experimental apparatus schematically sketched in Fig. 1. This setup is a modified configuration of that used in our previous [3,4] low energy experiments and described in detail in Ref. [11]. It consists of a large ionization chamber (75 cm active length), with a 300-μm silicon detector in the back, and of a time-of-flight system, with a 100-cm-long flight path. Two microchannel plates MCP1 and MCP2 supply the start and stop signals for the time-of-flight measurement. The above-mentioned detectors are rigidly connected

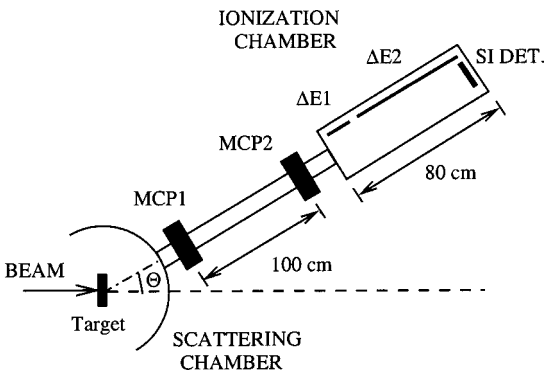

FIG. 1. Schematic view of the experimental apparatus.

†Deceased.

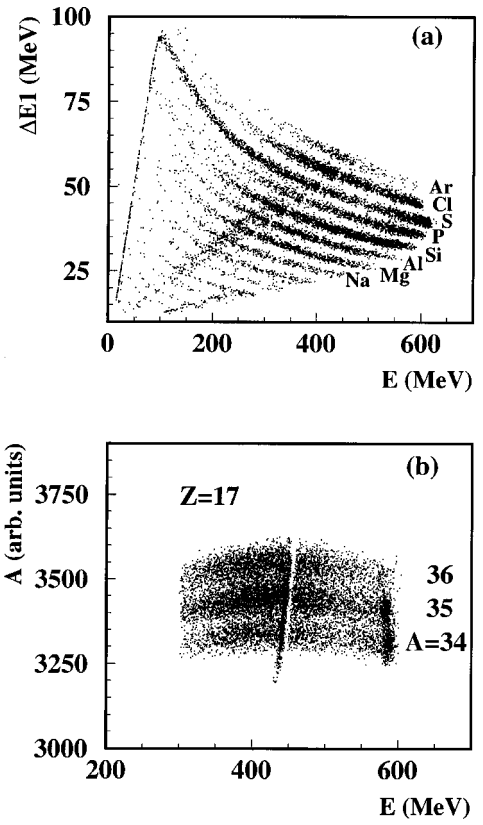

FIG. 2. (a) Energy loss in the first stage of the ionization chamber versus total energy, for the reaction products detected at the laboratory angle $\vartheta_L = 3°$. (b) Mass number A versus total energy for the reaction products with atomic number $Z = 17$, detected at the laboratory angle $\vartheta_L = 3°$.

to a sliding-seal scattering chamber which can be rotated around the target axis from $-10°$ to $+90°$ with reference to the beam line, allowing angular distribution measurements.

The ionization chamber operates with a steady flow of P10 mixture at a working pressure of about 300 torr. It is separated from the rest of the system, operating in high vacuum conditions, by means a 20-cm^2 surface window, made of a 4-μm-thick layer of polypropylene. The anode is divided into two sections, a ΔE_1 (15 cm length) and a ΔE_2 (60 cm length), which measure independently the energy loss of the detected ions. The silicon detector, placed at the end of the ionization chamber, gives the residual energy E_R of the detected ions punching through the chamber.

The energy loss information and the time-of-flight technique allow isotopic discrimination of the reaction products.

An overall energy resolution of about 0.6% was obtained at the elastic scattering energy, and the corresponding measured time resolution was approximately 200 ps [full width at half maximum (FWHM)]. Consequently, the expected mass resolution is about 2%.

An example of the detector performance is shown in Fig. 2. In part (a) the energy loss in the first stage of the ionization chamber is plotted as a function of the total energy of the reaction products, providing their charge identification. In part (b) the mass (obtained as energy times the square of the time of flight) of particles with atomic number $Z = 17$ is presented as a function of their total energy.

The energy and time calibrations of the detectors have been obtained from the elastic scattering of $^{32}S + ^{197}Au$ at $E(^{32}S) = 19.5$ MeV/nucleon at various angles. Some cuts in the time-of-flight spectrum of the diffused beam have also been used to improve the energy calibration.

For each identified reaction product we measured the angular distribution from $\vartheta_L = 2.5°$ to $\vartheta_L = 5°$, with $\Delta\vartheta_L = 0.5°$.

We also performed coincidence of heavy residues, detected by the ionization chamber, with α particles, detected by means of a telescope placed in the reaction plane inside the scattering chamber. The telescope, which can be positioned from 15° to 160° with respect to the beam direction, consists of three silicon surface-barrier detectors, 25, 100, and 3000 μm thick, respectively. In this way we can identify α particles with energy ranging from a few MeV to about 100 MeV.

Finally, in order to obtain relative normalization of the measured differential cross section, two 300-μm-thick silicon surface-barrier detectors were placed, as beam monitors, in the scattering chamber at $\pm 5°$ with respect to the beam axis.

The absolute normalization has been derived by comparing the elastic scattering data with the results of the optical model, calculated with the PTOLEMY code [12].

The error in the determination of the cross section includes the uncertainties in the left-right symmetry with respect to the beam axis, in the determination of the monitor angle, and in the normalization to the optical model results, resulting in an overall error of about 20%.

III. EXPERIMENTAL RESULTS AND ANALYSIS

A. Velocity spectra

We focused our attention on the evaporation residues to measure the contribution of complete and incomplete fusion, evaporation being the dominant decay mode for our system. For this reason we analyzed the reaction products having atomic charge number greater than 10, for which we expected contributions from complete fusion, according to the predictions of the statistical code LILITA [13] for this reaction.

In order to separate the complete fusion contribution from other reaction components, we performed a kinematical analysis of the invariant velocity spectra for each identified evaporation residue. The inclusive velocity spectra were obtained directly from the time-of-flight measurements.

In Fig. 3 we show, as a representative example, the inclusive invariant velocity spectra of separated individual charges (from $Z = 11$ to $Z = 18$), detected at $\vartheta_L = 3°$. In Fig. 4 the analogous spectra are reported, as an example, for the resolved masses in the case of $Z = 13$ and $Z = 17$. In these figures the histograms represent the experimentally measured differential cross section $d^2\sigma/d\Omega dV$ divided by V^2.

The complexity of the experimental spectra structure shows that different reaction mechanisms have to be considered. We assumed that the processes that contribute significantly to the observed residue yield are complete fusion, in-

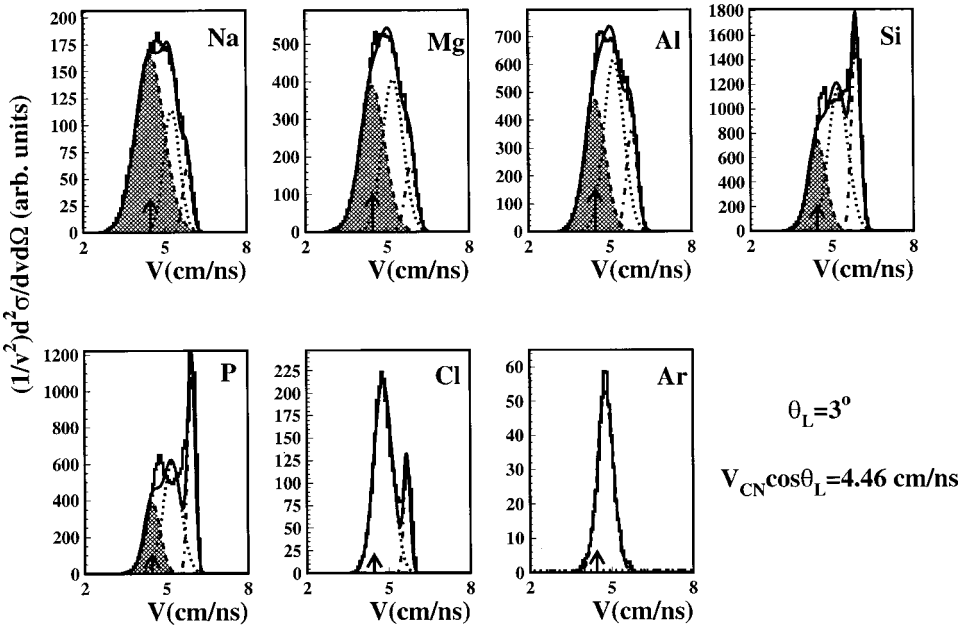

FIG. 3. Invariant velocity spectra of separated charges with Z ranging from 11 to 18, detected at $\vartheta_L=3°$. Histograms represent the data. The arrow marks the compound nucleus velocity at the detection laboratory angle, $V_{CN}\cos\vartheta_L$. The Gaussian distributions used to fit the data are presented as a dashed line (gray filled area) for the complete fusion component, as a dotted line for the incomplete fusion component, and as a dash-dotted line for the direct component. The solid line is the convolution of the three distributions.

complete fusion, and direct reaction.

The arrow in Fig. 4 indicates the compound nucleus velocity at the detection laboratory angle $V_{CN}\cos\vartheta_L$, thus giving the position of the complete fusion contribution in the velocity spectra. Since we study the system in reverse kinematics, the contribution with a velocity larger than $V_{CN}\cos\vartheta_L$ is to be ascribed to incomplete momentum transfer due to the fusion of the projectile with only a part of the target. Finally, direct reaction products will be located around the beam velocity $V_{beam}=6.15$ cm/ns.

Deep inelastic (DI) processes should also be considered, as their contribution may be not negligible at this bombarding energy. Moreover, in our system, the projectilelike DI products could have mass and charge similar to the evaporation residues. According to reaction kinematics this contribution should present two peaks in the velocity distribution, symmetric with respect to the $V_{CN}\cos\vartheta_L$ and whose positions depend on the Coulomb energy of the different possible DI channels and on the detection angle. The higher velocity peak could thus contaminate our incomplete fusion contribution, while the lower velocity one should be found on the left side of the complete fusion contribution. Simple calculations show that in any case the latter peak should occur at a velocity not exceeding the value of 4 cm/ns. None of the invariant velocity spectra, at any angle and for any residue, shows evidence of a contribution at such a low velocity. Furthermore, if we look at the targetlike fragments at forward angles, their contribution is quite small ($<5\%$) with respect to the total amount of residues. Assuming a symmetrical scenario, the contamination due to projectilelike fragments coming from deep inelastic processes should be of the same order.

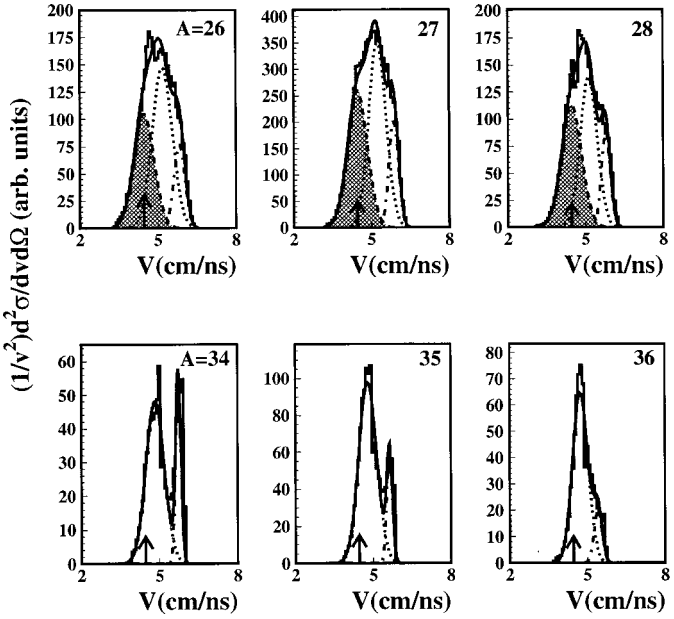

FIG. 4. Same as Fig. 3, but for the isotopically resolved masses in the case of $Z=13$ and $Z=17$.

In order to separate these different contributions we used a deconvolution technique, in which each reaction component was fitted with a Gaussian distribution. The convolution of these Gaussian curves is presented by the solid line in Figs. 3 and 4.

The Gaussian distribution used to fit the complete fusion component is theoretically obtained [14] assuming isotropic angular distributions in the c.m. system for all the emitted light particles. According to this assumption, the invariant velocity distribution of the evaporation residues originated in the complete fusion reaction has the following form:

$$\frac{1}{V^2}\frac{d^2\sigma}{d\Omega dV} = k\exp\left(-\frac{V_{CN}^2\sin^2\vartheta_L}{2s^2}\right) \times \exp\left[-\frac{(V-V_{CN}\cos\vartheta_L)^2}{2s^2}\right], \qquad (1)$$

in which $V_{CN}\cos\vartheta_L$ corresponds to the Gaussian centroid, s is the standard deviation, V is the laboratory velocity of the detected residue, and k is a normalization parameter.

In the fit procedure, we treat the calculated value of the Gaussian centroid $V_{CN}\cos\vartheta_L$ as a fixed parameter and allow the width s to be free to vary. We observed a smooth variation of s with the residues mass. In Figs. 3 and 4, the obtained fit for the complete fusion contribution is represented by the gray filled area under the dashed line.

In this way, we found that the complete fusion component is present up to $Z=15$. Moreover, its contribution decreases with increasing charge of the residue, in agreement with the results of the statistical evaporation model used in the following section. By looking at the isotopically resolved velocity spectra we did not find any particular behavior depending on the mass of the residue.

We therefore observe that, while the complete fusion decreases, the contribution of the second reaction component is present for all the measured residue charges (up to $Z=18$) and is found to increase with the residue charge. This behavior is well understood considering the incomplete fusion process between the beam and part of the target: the consequent excitation energy is lower than in the complete fusion and the reduced evaporation leads to a larger value of Z in the residue. Even in this case no particular behavior is found in the mass resolved spectra.

The third component shows a rise and fall around $Z=16$ and, for the same charge, decreases with the mass of the residue, thus showing the typical behavior of a direct reaction process.

We fitted the second and third parts of the spectra with two Gaussian curves, letting both the centroid velocity and width vary as free parameters in the fit procedure.

The fit results (dotted and dash-dotted lines in Figs. 3 and 4, respectively) for the different masses give values of the velocities close to those predicted in the case of incomplete fusion and direct reaction processes.

A further confirmation of the presence of complete and incomplete fusion mechanisms could arise from exclusive measurements, namely, from the study of the coincidences between evaporation residues and alpha particles, as already done by other authors [15].

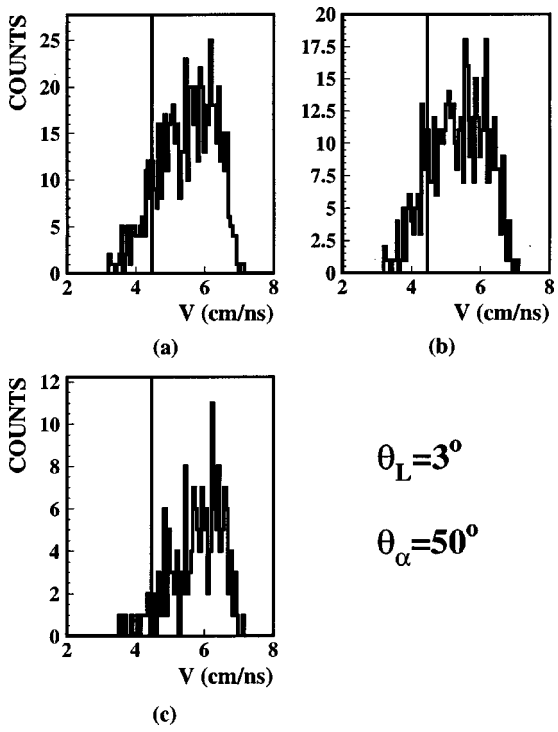

FIG. 5. Velocity distribution for all residues with charge from $Z=11$ to $Z=18$ (the $Z=16$ contribution is suppressed) detected at $\vartheta_L=3°$: (a) *inclusive* events, (b) coincidence events with alpha particles with energy from 15 to 120 MeV, and (c) coincidence events with alpha particles with energy from 4 to 15 MeV. The line marks the compound nucleus velocity at the detection laboratory angle, $V_{CN}\cos\vartheta_L$.

Low statistics of the coincidence events does not allow an analysis of the invariant velocity spectra with and without the trigger of alpha particle coincidences. Thus, we performed this analysis in terms of a plain velocity distribution and combining together all residues with atomic number from $Z=11$ to $Z=18$, except $Z=16$ which suffers from contamination by the scattered beam.

We present the obtained spectrum in Fig. 5(a), for 20 000 *inclusive* (i.e., no coincidences with alpha particles) events detected at $\vartheta_L=3°$. It clearly shows a component at compound nucleus velocity (marked by the line) and other components, already seen in the invariant velocity spectra, at a higher velocity.

Turning on the coincidence with 15–120 MeV alpha particles detected at $\vartheta_\alpha=50°$ does not modify the shape of the distribution, as shown in Fig. 5(b). This confirms that these alpha particles are evaporated from systems formed in complete and incomplete fusion processes.

On the contrary, the shape of the velocity distribution changes for the events in coincidence with lower energy (4–15 MeV) alpha particles, as shown in Fig. 5(c), where the compound nucleus contribution is reduced. This behavior confirms the higher velocity events as coming from the incomplete fusion process, in which the alpha particle is the remnant of the target and is therefore detected at very low

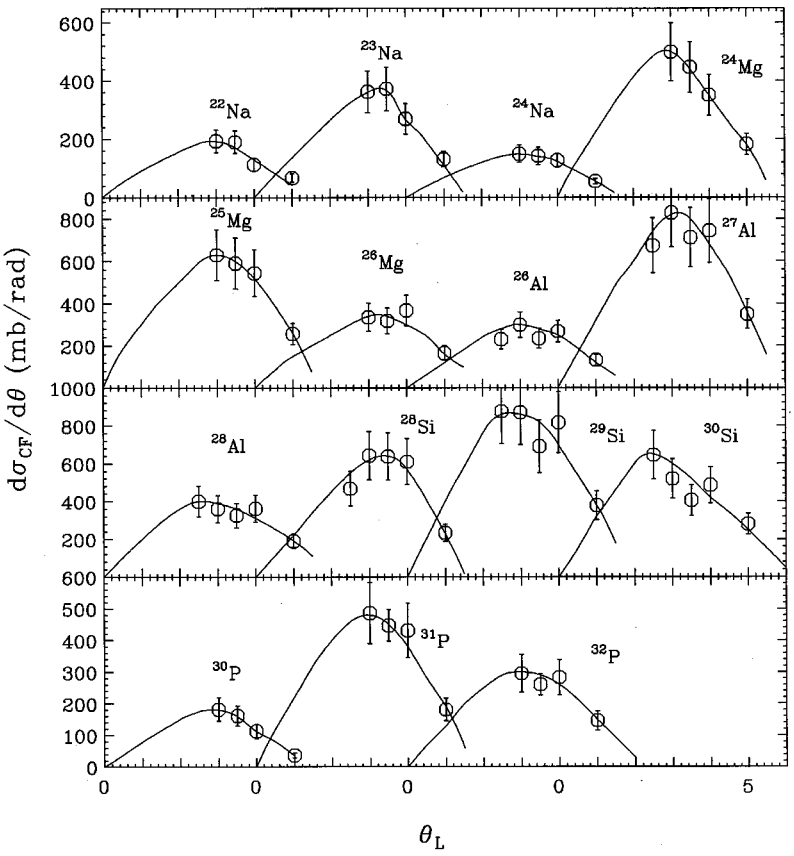

FIG. 6. Differential angular distributions of the residues coming from complete fusion. The lines are polynomial fits providing integrated cross sections.

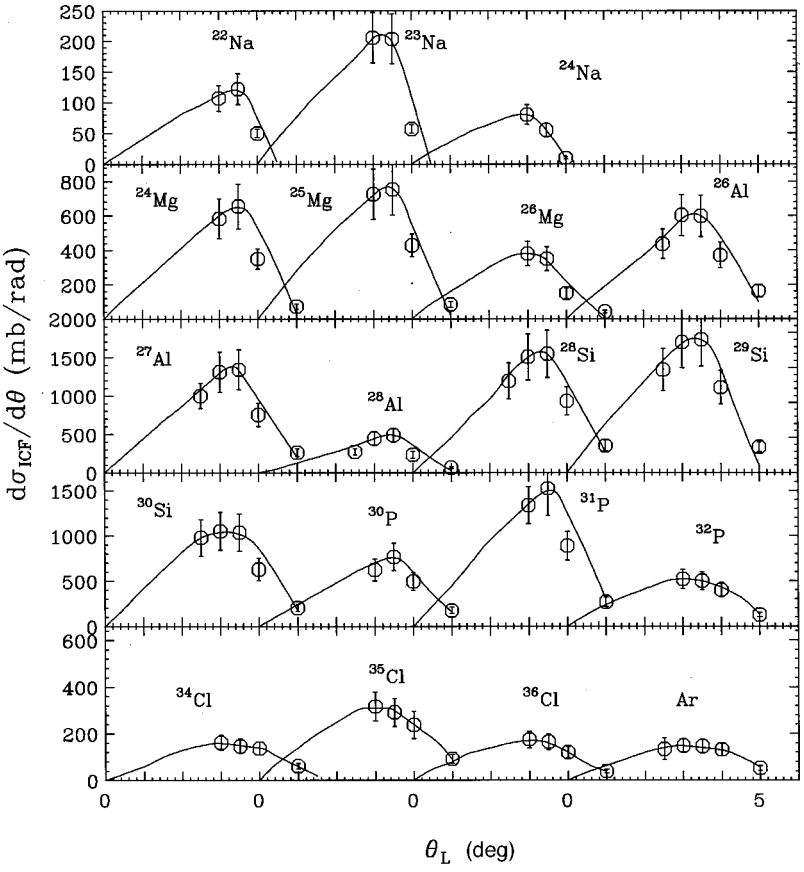

FIG. 7. Same as Fig. 6, but for the products coming from incomplete fusion.

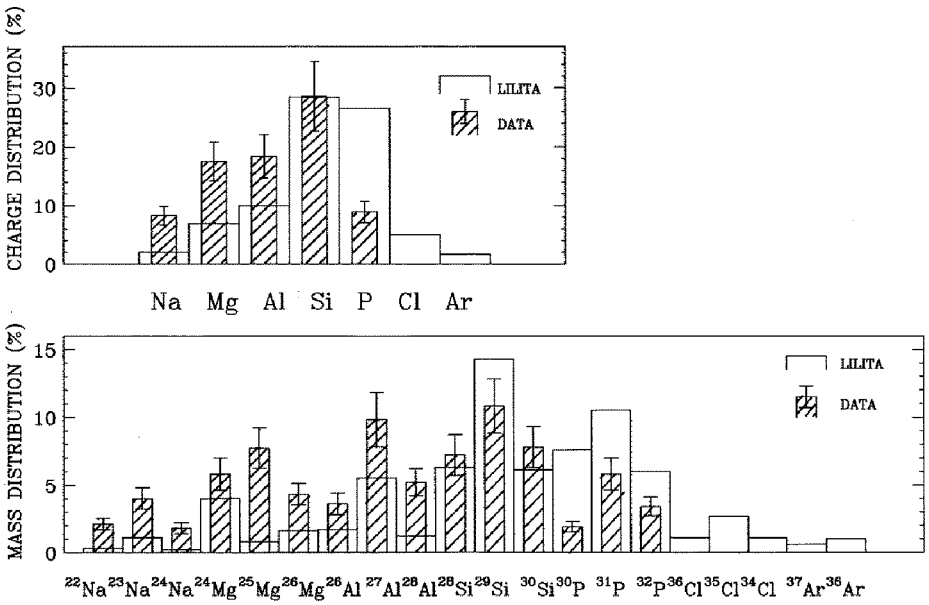

FIG. 8. Experimental relative charge and mass yields of the fusion residues (hatched bars) compared with LILITA calculations (open histograms).

energy. In fact, simple kinematical calculations, as well as a simulation performed with the code LILITA, show that particles with such a low energy are unlikely to come from the evaporation of our compound system, even in the backward direction in the center of mass.

B. Angular distributions

The differential angular distributions of the residues formed by complete and incomplete fusion in the $^{32}S+^{12}C$ reaction at $E(^{32}S)=19.5$ MeV/nucleon are shown in Figs. 6 and 7, respectively.

By integrating these distributions, we obtain the absolute cross sections for complete (σ_{CF}) and incomplete fusion (σ_{ICF}). Partial and total cross sections are listed in Table I, with their estimated errors. The major source of error in the determination of these cross sections arises from the data normalization, as discussed in Sec. II. Other sources of error reflect the experimental data statistics and the uncertainty in fitting the angular distributions, including extrapolation to smaller and larger angles.

We point out that the contribution of the ^{32}S evaporation residue to the complete fusion cross section has not been experimentally determined because of the intense background present in the ^{32}S spectrum. The fusion cross section contribution of this residue reported in Table I is that predicted by code LILITA for the studied reaction.

IV. COMPARISON WITH THEORY AND DISCUSSION

We compared the experimental data with the theoretical predictions of the statistical code LILITA. In Fig. 8, we report the experimental relative mass and charge yields of the complete fusion residues (hatched bars) and the results of the LILITA calculations (open histograms).

The predicted distributions appear shifted to larger mass and charge values with respect to the experimental one; this disagreement, already found in other works [16,17], can be interpreted as proof of heavy particle ($Z\geqslant 3$) emission, not included in the evaporation code.

The ratio of the extracted complete fusion cross section to the sum of complete and incomplete fusion cross sections is compared to the trend established by the systematics of Morgenstern *et al.* [6]. In that work this ratio is studied as a

TABLE I. Values of complete (σ_{CF}) and incomplete (σ_{ICF}) fusion cross sections for each evaporation residue. The reported value for ^{32}S represents the cross section predicted by the evaporation code LILITA. In the last row we report the total fusion cross section obtained summing the experimental data and the result of LILITA calculation.

	σ_{CF} (mb)	σ_{ICF} (mb)
^{22}Na	11± 2	5.3± 1
^{23}Na	20± 4	9± 1.8
^{24}Na	9± 2	3.4± 0.7
^{24}Mg	29± 6	32± 6
^{25}Mg	39± 8	38± 8
^{26}Mg	22± 4	19± 4
^{26}Al	18± 4	30± 6
^{27}Al	49±10	67± 13
^{28}Al	26± 5	24± 5
^{28}Si	36± 7	87± 17
^{29}Si	55±10	96± 19
^{30}Si	39± 8	58± 12
^{30}P	10± 2	38± 8
^{31}P	29± 6	76± 5
^{32}P	20± 4	30± 6
^{34}Cl		9.6± 2
^{35}Cl		18± 3.6
^{36}Cl		9.7± 2
Ar		9± 1.8
$\Sigma\sigma$	412±82	660±150
^{32}S	93	
$\Sigma\sigma+\sigma(^{32}S)$	505±82	660±150

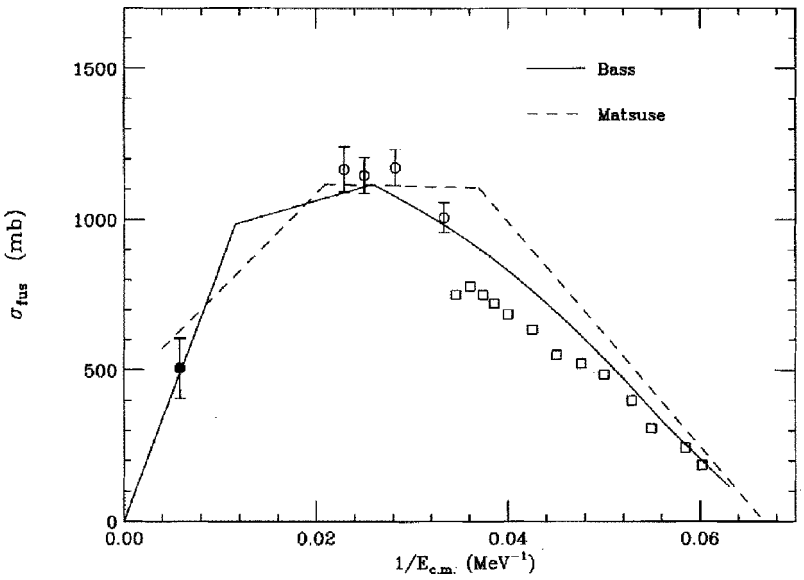

FIG. 9. Complete fusion cross section for the $^{32}S+^{12}C$ system as a function of $E_{c.m.}^{-1}$. Open squares are taken from Ref. [1]; open circles are our data at lower energies [2–4]. The solid circle is the result of this work. The dashed and solid lines are predictions of the critical distance fusion model of Matsuse *et al.* [18] and of the Bass model [9], respectively.

function of the velocity of the light partner nucleus of the reaction, v_L/c, for systems with different symmetry degree. The obtained value of 0.43 ± 0.13 agrees with the systematics for asymmetric systems, which gives, for the v_L/c of the presently studied system, a value of 0.36.

In Fig. 9, we show the experimental $^{32}S+^{12}C$ fusion cross sections available to date, as a function of $E_{c.m.}^{-1}$. The solid circle is the result from the present work. The dashed and solid lines are predictions of the critical distance fusion model of Matsuse *et al.* [18] and of the Bass model [9], respectively.

In the framework of the critical distance model of Matsuse *et al.*, the rapid drop of σ_{CF} at higher energies is interpreted in terms of a parametrized effective barrier at the critical distance between the colliding heavy ions (fusion entry line). The fusion cross section is evaluated in the three different energy regions by means of the following expressions:

region I (low energy region)

$$\sigma_{CF}^{I}=\pi R_B^2\left(1-\frac{V_B(R_B)}{E_{c.m.}}\right),$$

region II (central energy region)

$$\sigma_{CF}^{II}=\left(\frac{\pi I}{\mu}\right)\left[1+\frac{Q-\Delta Q}{E_{c.m.}}\right],$$

region III (high energy region)

$$\sigma_{CF}^{III}=\pi\langle d^2\rangle\left(1+\frac{\left[\frac{1}{2}\mu\omega_d^2\langle d^2\rangle-U_C[(<d^2>)^{1/2}]+Q\right]}{E_{c.m.}}\right),$$

where $(\langle d^2\rangle)^{1/2}$ is the critical distance between the colliding nuclei.

In the present calculations, the following parameters were used: for σ_{CF}^{I}, $V_B(R_B)=V_C(R_C)=Z_1Z_2e^2/R_C$, $R_C=R_0+\Delta R_C$, $R_B=R_0+\Delta R_B$, with $R_0=R_1+R_2$, $R_i=1.12A_i^{1/3}-0.86A_i^{-1/3}$, $\Delta R_B=2.70$ fm, and $\Delta R_C=3.70$ fm. For σ_{CF}^{II}, $I=2/3\,AM\langle r^2\rangle_A\alpha$, where M is the nucleon mass, $\langle r^2\rangle_A=3/5(1.12A^{1/3})^2(1+3.84A^{-2/3})$, $\alpha=0.87$, and $\Delta Q=12$ MeV. For σ_{CF}^{III}, $\omega_d=\beta\omega$, with $\omega=40A^{-1/3}/\hbar$ and $\beta=0.75$. The values of the parameters used are within the predicted limits reported in [18].

On the other hand, the Bass model reproduces the high energy fusion cross section behavior by using an empirical nuclear potential, obtained in the framework of the liquid-drop model, and some geometrical arguments. The nuclear part of the nucleus-nucleus potential of this model can be written as

$$V_n(s)=\frac{R_1R_2}{R_1+R_2}g(s),$$

where

$$g(s)=[A\exp(s/d_1)+B\exp(s/d_2)]^{-1}.$$

The parameters used in our calculations are those reported in Ref. [9], based on a global fit to fusion data, i.e., $A=0.03$ MeV^{-1} fm, $B=0.006$ MeV^{-1}, $d_1=3.30$ fm, $d_2=0.65$ fm, and $R_i=1.16A_i^{1/3}-1.39A_i^{-1/3}$.

Our previous [2–4] data appear to be in a satisfactory agreement with the predictions of Bass and Matsuse in energy region II, while in region III the Bass model seems to be closer to the present result. In region I, both calculations predict a higher fusion cross section than the experimental data [1].

From the complete fusion cross section we extracted, in the sharp cutoff approximation, the critical angular momentum l_{cr}, obtaining $l_{cr}=32\hbar$.

In Fig. 10, we report the excitation energy as a function of l_{cr} for the fusion of several systems. The data refer to $^{32}S+^{12}C$ [1–4], $^{20}Ne+^{24}Mg$ [19], and $^{16}O+^{28}Si$ [20,21] systems, leading to the same compound nucleus ^{44}Ti; our

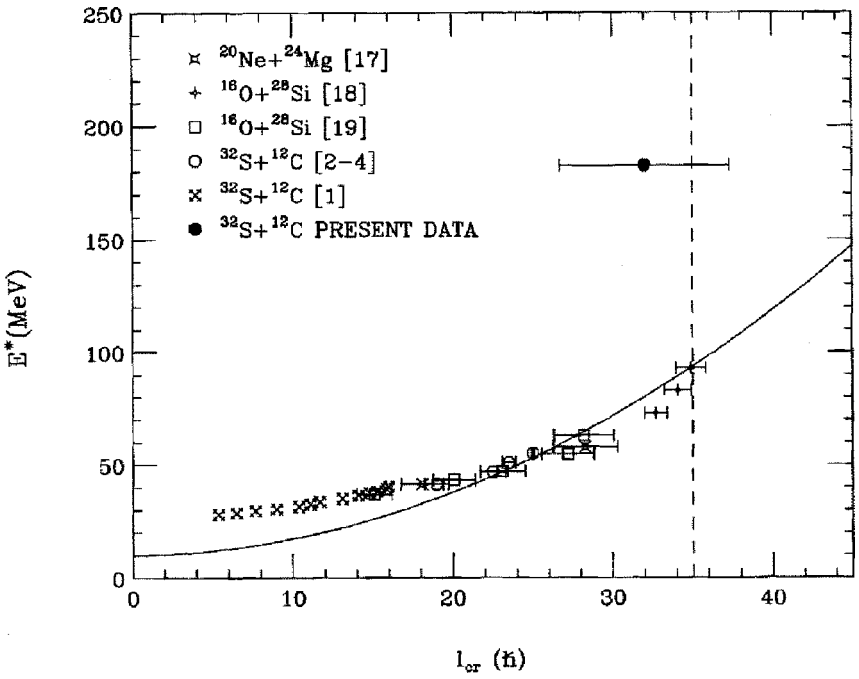

FIG. 10. Critical angular momentum extracted from complete fusion reactions at different excitation energies, leading to the same compound nucleus ^{44}Ti. The solid curve corresponds to the statistical yrast line [22]. The dashed line indicates the fission barrier limit of the compound nucleus according to the Sierk model [23,24].

present and previous results are reported as circles. The uncertainty in the l_{cr} values is due to the experimental error in the fusion cross section.

The solid line shown in the figure represents the statistical yrast line [22], calculated with $r_0=1.2$ fm and $\Delta Q=10$ MeV. The trend of the experimental data appears to be in good agreement with this model, in which the compound nucleus effects determine the behavior of the fusion excitation function.

The present data show a saturation in the critical angular momentum and the obtained value agrees with the calculated Sierk [23,24] fission barrier limit of the ^{44}Ti compound nucleus, represented by the vertical line in Fig. 10 ($l_{cr}^{th}=35\hbar$).

V. CONCLUSIONS

We have presented mass, charge, and angular distributions for the evaporation residues produced in the reaction ^{32}S $+^{12}$C at the energy $E(^{32}\mathrm{S})=19.5$ MeV/nucleon.

A kinematical analysis of the velocity spectra coupled to a deconvolution technique allowed us to separate different reaction components. The contributions found have been interpreted as originating from complete fusion, incomplete fusion, and direct reaction mechanisms. The obtained complete and incomplete fusion cross sections agree with previously established systematics [6], which correlate the fraction of incomplete fusion with the velocity of the lighter reaction partner and with the mass asymmetry in the entrance channel.

The discrepancy between the experimental relative mass and charge yields of the complete fusion residues and the LILITA predictions may be proof of heavy particle emission.

The experimental excitation function constructed using our present data, as well as our previous ones and those available in the literature, is in good agreement with the theoretical predictions derived in the framework of the Bass liquid-drop model interpretation, described in Ref. [9].

The critical angular momentum extracted from the fusion cross section for the studied reaction is consistent with the calculated Sierk [23,24] fission barrier limit of the ^{44}Ti compound nucleus. This result could indicate the existence of a limitation imposed by compound nucleus effects on the fusion cross section value.

However, in order to confirm the trend of the critical angular momentum, additional measurements are required for other systems leading to the same compound nucleus ^{44}Ti at excitation energies $E^*(^{44}\mathrm{Ti})>100$ MeV.

ACKNOWLEDGMENTS

We would like to thank the Laboratori Nazionali del Sud accelerator staff for their assistance in providing the beam during the experiment. We also thank V. Campagna, S. Salomone, and S. Urso for their technical help during the measurements, and Prof. S. Costa for a careful reading of the manuscript.

[1] J. J. Kolata, R. A. Racca, P. A. De Young, E. Aguilera-Reyes, and M. A. Xepses, Phys. Rev. C **32**, 1080 (1985).

[2] R. Giordano, F. Porto, S. Sambataro, and A. Scalia, Nuovo Cimento A **77**, 135 (1983).

[3] N. Arena, Seb. Cavallaro, S. Sambataro, S. Feminó, F. Porto, A. Anzalone, and P. Figuera, Nuovo Cimento A **100**, 953 (1988).

[4] N. Arena, Seb. Cavallaro, S. Feminó, P. Figuera, S. Pirrone, F.

Porto, and S. Sambataro, Phys. Rev. C **44**, 1947 (1991).
[5] B. A. Harmon, S. T. Thornton, D. Shapira, J. Gomez del Campo, and M. Beckerman, Phys. Rev. C **34**, 552 (1986).
[6] H. Morgenstern, W. Bohne, W. Galster, K. Grabisch, and A. Kyanowski, Phys. Rev. Lett. **52**, 1104 (1984).
[7] U. Mosel, in *Heavy Ion Collision*, edited by R. Bock (North-Holland, Amsterdam, 1979), Vol. II, pp. 45–126.
[8] D. E. Di Gregorio, J. Gomez del Campo, Y. D. Chan, J. L. C. Ford, Jr., D. Shapira, and M. E. Ortiz, Phys. Rev. C **26**, 14 (1982); M. Diebel, D. Glas, U. Mosel, and H. Chandra, Nucl. Phys. **A333**, 253 (1980); S. M. Lee, T. Matsuse, and A. Arima, Phys. Rev. Lett. **45**, 165 (1980); R. Vandenbosch and A. J. Lazzarini, Phys. Rev. C **23**, 1074 (1981).
[9] R. Bass, Phys. Rev. Lett. **39**, 265 (1977).
[10] R. Bass, *Nuclear Reaction with Heavy Ions* (Springer-Verlag, New York, 1980), pp. 267, 318–369; J. R. Birkelund, L. E. Tubbs, and J. R. Huizenga, Phys. Rep. **56**, 107 (1979).
[11] P. Figuera, S. Pirrone, A. Anzalone, N. Arena, Seb. Cavallaro, S. Feminó, F. Giustolisi, F. Porto, and S. Sambataro, Nuovo Cimento A **104**, 251 (1991).
[12] M. H. Farlane and S. C. Poeper, Argonne National Laboratory Report No. ANL-76-11, 1978.
[13] J. Gomez del Campo and R.G. Stokstad, ''LILITA, a Monte Carlo Statistical Model Code,'' Oak Ridge National Laboratory Technical Memo No. ORNL-TM-7295, 1981.
[14] J. Gomez del Campo, R. G. Stokstad, J. A. Biggerstoff, R. A. Dayras, A. H. Snell, and P. H. Stelson, Phys. Rev. C **19**, 2170 (1979).
[15] H. Morgenstern, W. Bohne, W. Galster, and K. Grabisch, Z. Phys. A **324**, 443 (1986).
[16] M. F. Vineyard, J. S. Bauer, J. F. Crum, C. H. Gosdin, R. S. Trotter, D. G. Kovar, C. Beck, D. J. Henderson, R. V. F. Janssens, B. D. Wilkins, C. F. Maguire, J. F. Mateja, F. W. Prosser, and G. S. F. Stephans, Phys. Rev. C **45**, 1784 (1992).
[17] G. P. Gilfoyle, M. S. Gordon, R. L. McGrath, G. Auger, J. M. Alexander, D. G. Kovar, M. F. Vineyard, C. Beck, D. J. Henderson, P. A. DeYoung, and D. Kortering, Phys. Rev. C **46**, 265 (1992).
[18] T. Matsuse, A. Arima, and S. M. Lee, Phys. Rev. C **26**, 2338 (1982).
[19] K. Grotowski, P. Belery, Th. Delbar, Y. ElMasry, Gh. Gregoire, R. Janssens, J. Vervier, G. Paic, M. Albinska, S. Albinski, S. Kupta, T. Kozic, and R. Planeta, Phys. Rev. C **23**, 2513 (1981).
[20] R. A. Zingarelli, L. C. Dennis, M. A. Tiede, R. C. Kline, K. W. Kemper, and S. V. Mitchell, Phys. Rev. C **48**, 651 (1993).
[21] R. Rascher, W. F. J. Muller, and K. P. Lieb, Phys. Rev. C **20**, 1028 (1979).
[22] S. M. Lee, T. Matsuse, and A. Arima, Phys. Rev. Lett. **45**, 165 (1980).
[23] Arnold J. Sierk, Phys. Rev. C **33**, 2039 (1986).
[24] S. J. Sanders, Phys. Rev. C **44**, 2676 (1991).